ACS APPLIED MATERIALS & INTERFACES

www.acsami.org

Research Article

Highly Strong and Solvent-Resistant Cellulose Nanocrystal Photonic Films for Optical Coatings

Fusheng Zhang, Wenna Ge, Cunli Wang, Xintong Zheng, Dongdong Wang, Xiancheng Zhang, Xue Wang, Xingya Xue, and Guangyan Qing*

Cite This: *ACS Appl. Mater. Interfaces* 2021, 13, 17118–17128

Read Online

ACCESS | Metrics & More | Article Recommendations | Supporting Information

ABSTRACT: Cellulose nanocrystals (CNCs) are powerful photonic building blocks for the fabrication of biosourced colored films. A combination of the advantages of self-assembled CNCs and multiple templating agents offers access to the development of novel physicochemical sensors, structural coatings, and optic devices. However, due to the inherent brittleness and water instability of CNC-derived materials, their further applications are widely questionable and restrictive. Here, a soft polymer of poly(vinyl alcohol) (PVA) was introduced into the rigid CNC system to balance molecular interactions, whereafter two hard/soft nanocomposites were fastened through a cross-linking reaction of glutaraldehyde (GA), resulting in a highly flexible, water-stable, and chiral nematic CNC composite film through an evaporation-induced self-assembly technique. For a 1.5 wt % GA-cross-linked 70 wt % CNC loading film, its treatment with harsh hydrophilic exposure (soaking in a strong acid, strong base, and seawater) and various organic solvents show exceptional solvent-resistant abilities. Furthermore, the film can even withstand a weight of 167 g cm^{-2} without failure, which is a highly stiff and durable character. Importantly, the film remains a highly ordered chiral nematic organization, being able to act as a highly transparent substrate for selective reflection of left-handed circularly polarized light, preparing fully covered and patterned full-color coatings on various substrates. Our work paves the way for applications in low-cost, durable, and photonic cellulosic coatings.

KEYWORDS: *cellulose nanocrystal, toughness, solvent resistance, circularly polarized light, coatings*

INTRODUCTION

Cellulose is an excellent cost-effective resource to construct multifarious layered photonic structures, relying on multitype cellulose-based nanosized building blocks (i.e., hydroxypropyl cellulose, ethylcellulose, and cellulose nanocrystal).[1−4] Cellulose nanocrystals (CNCs) are one of the most representative objects, which can be ordinarily used as liquid-crystal templates to construct various photonic nanostructured solid films.[5] In terms of their appealing optical and structural properties, CNCs have potential application in structural coatings,[6,7] optical devices,[8,9] physical or chemical sensings,[10,11] imaging with circularly polarized light, and also plasmonics.[12,13] However, these photonic CNC materials are widely questionable for being inherently susceptible to water and prone to cracking, remarkably limiting their performance on an application in practice. Especially, CNC composite films are seldom applied straightforward in biological fields. For instance, a self-healing chiral photonic CNC film would either swell or shrink in polar solvents (e.g., water, ethanol, and dimethylformamide (DMF)) with a remarkable impact on their sensing properties.[14] The reasons for these limitations are[15,16] (1) a lack of an appropriate binder phase to balance energy dissipation of the rigid CNCs and thus influence the structural integrity and (2) cellulosic materials comprising highly hydrophilic β-(poly-1,4-D-glucose) units, causing their solid films to usually swell in water. Until now, a convenient strategy for the fabrication of a flexible, water-stable, and optically functional CNC material system remains a challenge.

A bioinspired strategy is a powerful method for the pursuit of high-performance materials.[17−20] Chameleons enable vivid color change by adjusting the packed array of guanine crystals within a layer of dermal iridophores (Figure 1a). Therein, neurocontrolled soft tissue cells drive active tuning of hard photonic crystals, providing reversible color change and efficient elastic deformation.[21] Inspired by this ordered soft/hard nanoarchitecture, Kim's groups[22] designed stretchable photonic films composed of a regular array of silica particles and an acrylate elastomer. Based on this biomimetic strategy, it is possible to achieve flexible functions for CNC-derived

Received: February 9, 2021
Accepted: March 24, 2021
Published: April 1, 2021

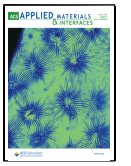

https://doi.org/10.1021/acsami.1c02753
ACS Appl. Mater. Interfaces 2021, 13, 17118−17128

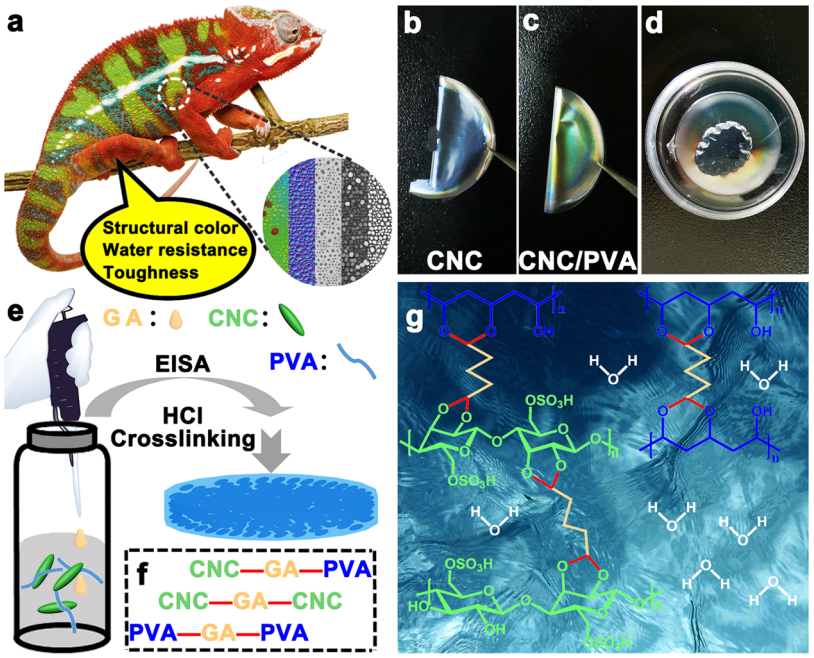

Figure 1. Design concept of a durable and solvent-resistant cellulose nanocrystal (CNC) film. (a) Chameleon skins are composed of close-packed guanine nanocrystals embedded in multifunctional superimposed iridophores that form an advanced photonic nanostructure, which makes chameleons generate highly flexible, durable, and reversible structural colors (reproduced from Teyssier et al.[21]). (b) Brittle CNC film. (c, d) Inspired by the mechanism of chameleons, a highly flexible CNC film was prepared through the introduction of 30 wt % soft poly(vinyl alcohol) (PVA); however, this composite film is unstable in water and swells easily (d). (e) Schematic illustration of the preparation process of a glutaraldehyde (GA) cross-linked CNC/PVA film for the improvement of mechanical strength and water stability through an evaporation-induced self-assembly (EISA) technique. (f) Multiple complexations between CNC and PVA cross-linking through GA. (g) Possible formation mechanism of the polymer network within CNC/PVA-GA.

photonic materials. A representative report of Walther's groups demonstrated the combination of hard CNCs with soft poly(vinyl alcohol) (PVA) to enhance the ductility of photonic CNC materials.[16] Soon afterward, based on this bioinspired reinforced method, a series of soft polymers were composited with CNCs to fabricate multifunctional photonic materials. For instance, Tsukruk's[23] and Zhang's[24] groups recently created highly flexible chiral luminescence security patterns from the co-assembly of CNCs, soft poly(ethylene glycol) (PEG) or PVA polymers, and carbon dots through soft lithography and the mold technique. Furthermore, this co-assembled strategy has found wide applications in other CNC composites, such as responsive actuators,[25] advanced smart textiles,[26] and colorimetric sensors.[27,28] However, these flexible CNC-derived photonic hybrid materials could be easily disrupted by water, which results in the collapse of chiral self-assembled structures, thus easily causing the loss of optical activities. Some attempts reported sophisticated modification of CNCs with elastomers to enhance the material flexibility and water resistance through a combination of CNCs and organic polymers, including acrylate copolymer and soft latex nanoparticles.[29,30] Nonetheless, these methods are tedious, time-consuming, and expensive for large-scale generation and hence limiting for multiple application processes, such as coating decoration. In contrast, a universal and easy-to-obtain approach for enhancing both the mechanical properties and the tolerance to polar solvents of CNC composites is quite appealing.

In this study, we report an advantage strategy for the fabrication of tough and water-stable photonic CNC composite films. Typical CNC solid films constitute the random assembly of tactoids, which is a highly defective structural organization, causing them to be unable to efficiently dissipate fracture energy and resulting in brittleness of the films.[31,32] PVA is cost-effective material because of the advantage of desirable degradability, tensile strength, flexibility, and adjustable molecular weight.[33,34] Hence, a certain proportion of soft PVA was introduced to improve the toughness of the CNC film, as previously reported by Walther.[16] The presence of the soft polymer acts as a plasticizing agent to slightly enhance the dissipative movement between the molecular interactions of the rigid CNCs. Nevertheless, the resulting photonic film could not make its photonic structure withstand high humidity and water environments. To overcome this shortcoming, subsequent treatment of CNC composites with GA chemical cross-linking fixed the two-phase polymers and further improved their mechanical property and water stability. Compared with pristine CNC and CNC/PVA films, a 70 wt % CNC loading film with GA cross-linking not only shows an excellent solvent resistance capability in multiple solvents but also has long-term durability. Excitingly, the GA-cross-linked CNC composite film remains a transparent substrate with prominent chiral nematic structures, enabling selective reflection of left-handed circularly polarized light. Furthermore, various flexible and solvent-resistant films with tunable iridescence could be prepared by varying the ionic strength of the solutions. Although structural color materials and pigments are of great interest in the field of photonic coatings,[35−37] tedious synthesis and purification increase the cost of production and limit large-scale production. By contrast, the photonic CNC composite film is a promising candidate for environmentally friendly photonic coatings. This strategy could be boldly extended to other photonic cellulosic materials, and this work may be potentially

https://doi.org/10.1021/acsami.1c02753
ACS Appl. Mater. Interfaces 2021, 13, 17118−17128

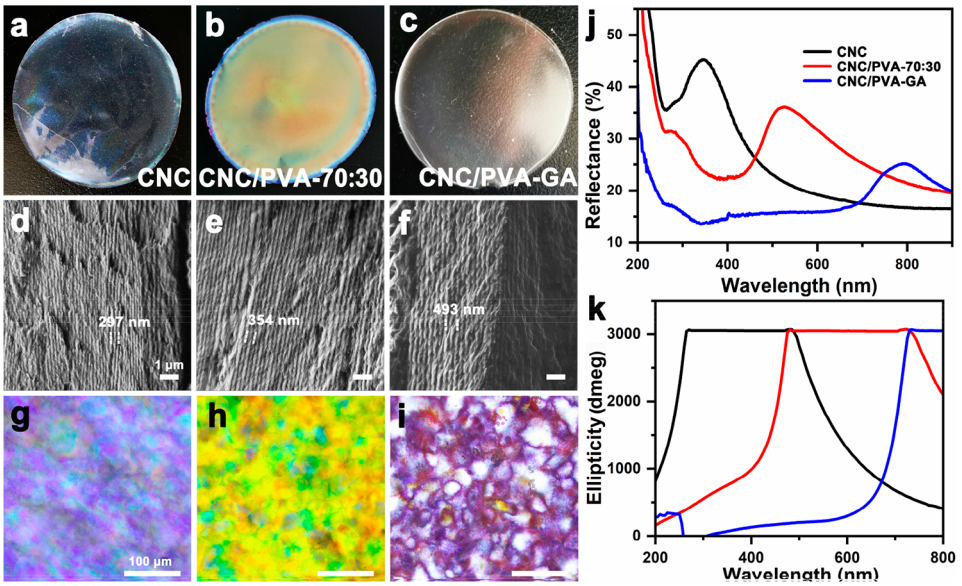

Figure 2. Photographs (a–c), cross-sectional scanning electron microscopy (SEM) images (d–f), and polarized optical microscopy (POM) images (g–i) of CNC (a, d, g), CNC/PVA-70:30 (b, e, h), and CNC/PVA-GA (c, f, i) films. Photographs of these films (diameter: 5 cm). Reflectance spectra (j) and circular dichroism spectra (k) of these films (thickness of approximately 40 μm).

applied to durable optics, signage, low-cost polarizers, and decorative patterns.

RESULTS AND DISCUSSION

The chiral nematic phase of CNCs can self-assemble into desired iridescent solid films and thereby allow for access to novel photonic materials.[38] First, to prepare a highly flexible CNC-based material, the influence of the PVA dosage on the rigidness of CNC composites was investigated by adjusting the mass ratios of CNC/PVA in a range from 100:0 to 30:70 (w/w, Figures S1 and S2). Among them, a 70 wt % CNC loading composite film (CNC/PVA-70:30) shows high flexibility (Figure 1c) and the strongest tensile property (104 ± 4 MPa, Table S1). The iridescent appearance of the CNC/PVA-70:30 film was attractive, but it was highly susceptible to water. When several droplets of water were dropped on the surface of CNC/PVA-70:30 for about 1 min (Figure 1d), the iridescence of the film disappeared gradually, which could be reasonably attributed to the swelling of the hydrophilic polymer chains, causing an excessive increase of pitch distance. This phenomenon indicated that the composite film was incompatible with humid and liquid environments. How to achieve flexibility and water stability for CNC-derived materials, just like chameleons, has been rarely reported. Here, we propose to construct an ideal cross-linked structure in the CNC matrix. The synthesis process is depicted in the schematic (Figure 1e). In a typical procedure, 2 wt % CNC suspension and a PVA solution in a 20 mL glass vial were mixed and stirred for 4 h at room temperature to form a homogeneous dispersion. The ratio of CNC/PVA is 70:30 by weight. Briefly, an optimal amount of 1.5 wt % GA was added dropwise into the above mixture and stirred for 12 h. The resulting suspension was then cast in a polystyrene Petri dish and dried for 72 h at 30 °C. After drying entirely, a freestanding film was immediately exposed to hydrochloric acid (HCl) vapor for 5 min, facilitating GA cross-linking. Finally, a water-stable, highly flexible, and chiral nematic CNC composite film (i.e., CNC/PVA-GA) was obtained. Due to the high aspect ratio of CNCs, PVA could entangle with CNC chains through multiple hydrogen-bonding interactions among the hydroxyls. After exposure to HCl vapor, the aldehydes of GA could form stable cyclic acetal bonds (Figure 1f,g) by cross-linking with PVA and/or CNC via the formation of three types of structures,[39,40] i.e., CNC-GA-PVA, CNC-GA-CNC, and PVA-GA-PVA. The detailed optimization process of the GA-cross-linked CNC/PVA-70:30 from 0.5, 1.0, and 1.5 to 2.0 wt % is shown in the Experimental Section.

As shown in Figure 2a–c, CNC, CNC/PVA-70:30, and CNC/PVA-GA films were iridescent in appearance from blue and orange to red by the naked eye. The physical color variation of these films can be explained by the following equation[41]

$$\lambda_{max} = n_{avg} \cdot P \tag{1}$$

where λ_{max} is the peak wavelength reflected by the chiral nematic structure at normal incident light, which is proportional to the average refractive index (n_{avg}) and the helical pitch (P) of chiral nematic materials. When PVA and GA cross-linking are introduced into the chiral nematic phase of the CNC system, they naturally cause the change of the reflected color in the chiral nematic structure. UV–vis spectra (Figure 2j) recorded the reflection peaks of CNC, CNC/PVA-70:30, and CNC/PVA-GA films, the peak wavelength of which are 345, 524, and 791 nm, respectively. Due to the introduction of PVA and GA, the photonic CNC shows an evident red shift in the reflection peak. According to the aforementioned equation, the red shift of λ_{max} is attributed to the increase of n_{avg} or P. n_{avg} may be calculated from volume fractions and refractive indices of the individual components according to the following equation[42]

$$n_{avg} = \sum_i V_i n_i \tag{2}$$

As the refractive indices of PVA and GA (n_{PVA} = 1.52, n_{GA} = 1.43) are less than that of CNC (n_{CNC} = 1.54), the n_{avg} of CNC/PVA-70:30 and CNC/PVA-GA slightly decreases and

https://doi.org/10.1021/acsami.1c02753
ACS Appl. Mater. Interfaces 2021, 13, 17118–17128

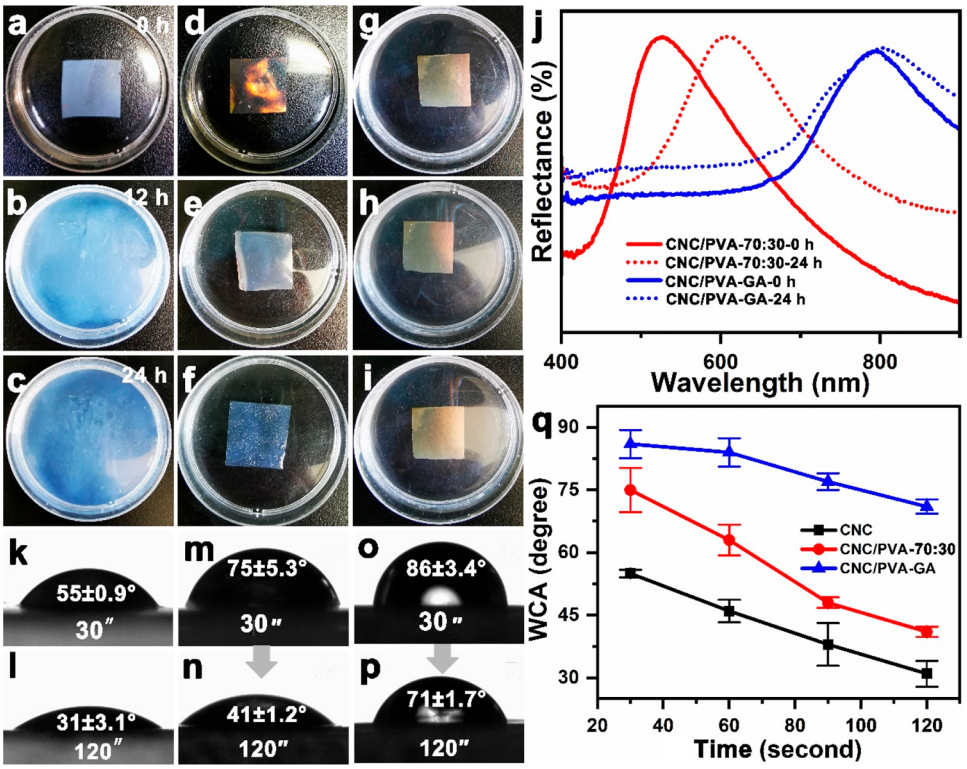

Figure 3. Comparison of the water stability of CNC (a–c), CNC/PVA-70:30 (d–f), and CNC/PVA-GA (g–i) films. These films are immersed in water for 0 h (a, d, g), 12 h (b, e, h), and 24 h (c, f, i), respectively. (j) Reflectance spectra of CNC/PVA-70:30 (blue) and CNC/PVA-GA (red) at 0 h (solid lines) and 24 h (dotted lines). Water droplet profiles on CNC (k, l), CNC/PVA-70:30 (m, n), and CNC/PVA-GA (o, p) films captured at 30 s (upper panel) and 120 s (lower panel), respectively. (q) Time-dependent water contact angle (CA) of the CNC (black), CNC/PVA-70:30 (red), and CNC/PVA-GA films (blue). Error bars represent the standard error of the mean for measurements carried out in triplicate.

the values are 1.51 and 1.49, respectively. Similar n_{avg} could not contribute to the alteration of the reflection peak, and therefore these red shifts might be caused by the increasing *P*. The *P* value is defined as the distance between two continuous interlayers of the fracture surface of chiral nematic materials, which can be observed using a scanning electron microscope (SEM). Figure 2d–f shows the cross-sectional microstructure of CNC, CNC/PVA-70:30, and CNC/PVA-GA. All of them display periodic layered structures but differ in the interlayer distances, and their *P* values are 297, 354, and 493 nm, respectively. The results explained that a considerable increase in the *P* value led to a substantial red shift in the reflection peak of the CNC/PVA-GA film.

Polarized optical microscopy (POM, Figure 2g–i) images of CNC, CNC/PVA-70:30, and CNC/PVA-GA demonstrate the typical characteristics of the chiral nematic organization. A remarkable difference in the strong birefringence and a shift in color from blue and yellow to dark red could be attributed to the introduction of PVA and GA. Furthermore, CNC, CNC/PVA-70:30, and CNC/PVA-GA present remarkably intense signal peaks of positive ellipticity in circular dichroism (CD) spectra (Figure 2k), confirming the left-handed chiral nematic structures in these films. A regular peak shift in the CD spectra was consistent with a similar change in the reflection peak observed by the UV–vis spectra. Taken together, these investigations revealed that the structural replication of the composite films arose from the chiral nematic phase of CNCs.

Incorporation of soft PVA and the cross-linked reaction into the pristine CNC film not only altered the reflections of the chiral nematic structure but also remarkably improved the solvent resistance of the material. In this test, CNC, CNC/PVA-70:30, and CNC/PVA-GA films were cut into small pieces with a size of 2 × 2 cm^2 and immersed in water to evaluate their water stability. During this process, the profiles of these test pieces were recorded by a camera at 0, 12, and 24 h, respectively, as shown in Figure 3a–i. It was found that the CNC film gradually swelled in water and completely dissolved after 12 h (Figure 3b). By comparison, CNC/PVA-70:30 presented a slow swelling behavior and a red shift occurred in the reflection (Figure 3d). Only after 24 h, the iridescent color disappeared and the area of the film increased by approximately 20% (Figure 3f) because of the swelling. Interestingly, CNC/PVA-GA retained its structural integrity and iridescence from 0 to 24 h (Figure 3g–i). No evidential change was observed when the composite film was immersed in water for another week. The swelling effect on the reflection peaks was measured through UV–vis spectra (Figure 3j), and an 83 nm red shift was detected in the reflection peaks (red lines) when the CNC/PVA-70:30 film was immersed in water for 24 h. In sharp contrast to this, the reflection peak of the CNC/PVA-GA film was well maintained (blue lines).

Wettability is an important surface parameter and strongly affects mass transport and functional applications. The experiment of wetness indicated that the CNC film was hydrophilic, which was attributed to lower crystallinity and surface amphiphilicity.[43,44] CNC and CNC/PVA-70:30 films showed static contact angles (CAs) of 55 ± 0.9° (Figure 3k) and 75 ± 5.3° (Figure 3m), respectively, at 30 s. After stabilization for 120 s, their CAs reduced to 31 ± 3.1° (Figure 3l) and 41 ± 1.2° (Figure 3n), respectively. We presumed that

https://doi.org/10.1021/acsami.1c02753
ACS Appl. Mater. Interfaces 2021, 13, 17118–17128

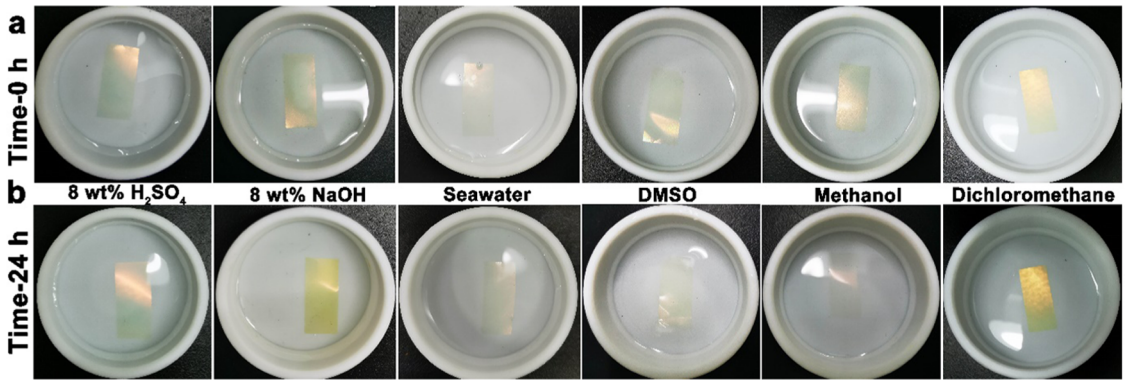

Figure 4. Photographs of CNC/PVA-GA films after being immersed in various solvents for 0 h (a) and 24 h (b) displaying satisfactory solvent resistance of the films.

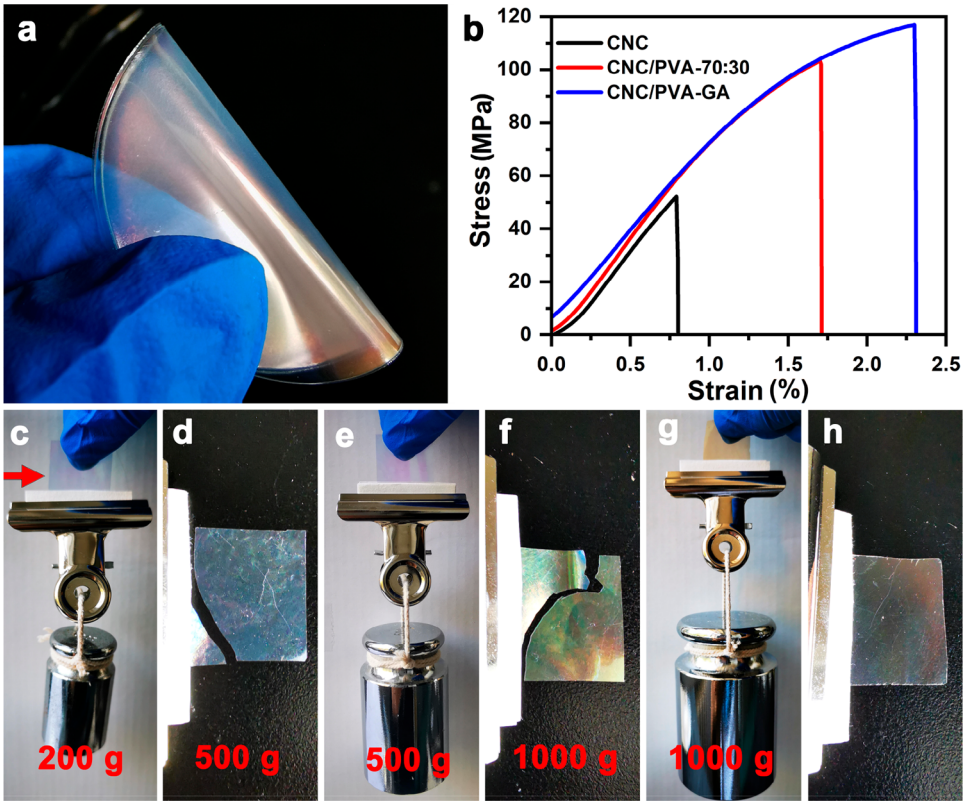

Figure 5. Mechanical characterization of CNC, CNC/PVA-70:30, and CNC/PVA-GA films. (a) Photograph of a flexible and iridescent CNC/PVA-GA film. (b) Stress−strain curves of these films. (c−h) Photographs of lifting-weight experiments (c, e, g) and the films after lifting (d, f, h); images from left to right correspond to CNC (c, d), CNC/PVA-70:30 (e, f), and CNC/PVA-GA (g, h) films.

water could penetrate these films and destroy the compact polymer networks quickly, leading to a sharp decrease in the CA. In contrast, the CNC/PVA-GA film has a larger initial CA of 86 ± 3.4° (Figure 3o) and its CA only decreased to 71 ± 1.7° (Figure 3p) at the identical time. Time dependence of CA changes (Figure 3q) further validated that CNC/PVA-GA had satisfactory water stability.

Further, CNC, CNC/PVA-70:30, and CNC/PVA-GA films were treated with harsher solvent environments for the evaluation of their solvent resistance (Figures 4 and S5); these films were immersed in H_2SO_4 (8 wt %), NaOH (8 wt %), seawater, dimethyl sulfoxide (DMSO), methanol, and dichloromethane, respectively, for 24 h. Neither pristine CNC nor CNC/PVA-70:30 could maintain its original appearance in these solvents (Figure S5). CNC films were completely dissolved in seawater and DMSO. CNC/PVA-70:30 films swelled in H_2SO_4, NaOH, seawater, and DMSO. However, it was very heartening to observe CNC/PVA-GA with its structural integrity and the characteristic iridescence from 0 to 24 h (Figure 4). Comparison of these results confirmed that the GA-cross-linked strategy could remarkably improve the structural stability of the photonic CNC composite films in various harsh solvent environments.

In addition to the solvent stability, photonic CNC composites with sufficient durability, flexibility, and structural toughening property are quite attractive as a promising nanocomposite coating in the modern green paint industry.[45,46] To overcome CNC brittleness, PVA additives were used to enhance its flexibility. To improve the water stability of CNC composites, GA cross-linking causes them not only to be

https://doi.org/10.1021/acsami.1c02753
ACS Appl. Mater. Interfaces 2021, 13, 17118−17128

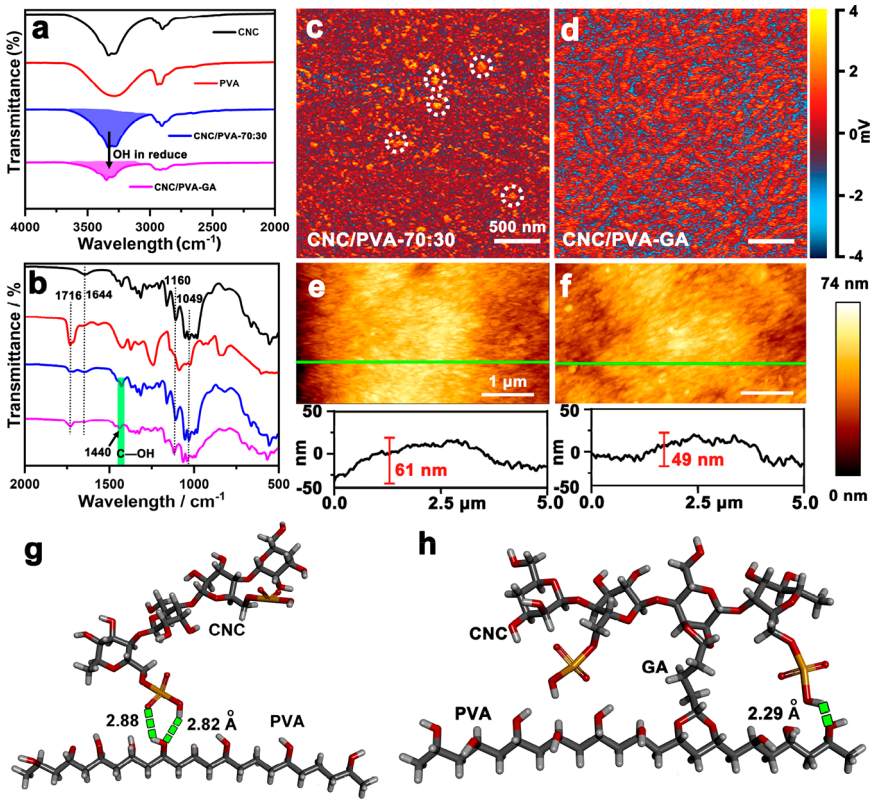

Figure 6. (a, b) Amplified FTIR spectra of CNC (black), PVA (red), CNC/PVA-70:30 (blue), and CNC/PVA-GA (violet) films. AFM-IR images of CNC/PVA-70:30 (c) and CNC/PVA-GA (d) films recorded at 1716 cm^{-1} (characteristic wavelength of the acetal bond) displaying different phasic distributions. (d) AFM height images of CNC/PVA-70:30 (e) and CNC/PVA-GA (f) films and the corresponding section profiles along the green lines. The calculated binding model of 11 fragments of CNC/PVA (g) and CNC/PVA-GA (h) obtained using quantum chemistry calculations (i.e., Gaussian and density functional theory (DFT) at a 6-311g level of theory).

solvent-resistant but also provides them with elasticity and toughness. Figure 5a shows a photograph of CNC/PVA-GA folded in half without cracking, implying that it is highly flexible. Utilizing a universal material testing machine equipped with a 20 N load cell, the mechanical tensile properties of the CNC, CNC/PVA-70:30, and CNC/PVA-GA films at the RHs (RH = relative humidity) of 50 and 80% were investigated,[16,27] and the results are summarized in Figures 5b and S6 and Table S2. CNC/PVA-GA had a tensile strength of 113 ± 6 MPa and a strain-to-failure of 2.3 ± 0.2%. These parameters were substantially higher than those of CNC and CNC/PVA-70:30 films (Figure 5b). CNC/PVA-GA had Young's modulus of 4.9 ± 0.5 GPa that was less than 5.8 ± 1.8 GPa of CNC and 7.1 ± 0.9 GPa of CNC/PVA-70:30 (Table S2). The tensile test of CNC and CNC/PVA-70:30 films in high humidity distinctly decreased, while CNC/PVA-GA still showed stable tensile property (Figure S6). In comparison, the tensile strength of the CNC/PVA-GA film was higher than those of previously reported CNC/polymers, including CNC/PVA,[16] CNC/PEG,[27] CNC/hydroxypropyl cellulose,[47] and CNC/polysaccharide composite films.[48] Besides, CNC/PVA-GA and CNC/these polymers had a similar value of strain-to-failure. This performance explained that the soft PVA and GA cross-linking in the CNC composite could provide more energy dissipation for the CNC layers, occurring in a distinct yielding and plastic deformation.[48,49]

A simple lifting-weight experiment could visualize the mechanical properties of CNC, CNC/PVA-70:30, and CNC/PVA-GA films, which were cut into rectangular pieces with a length of 30 mm, a width of 20 mm, and a thickness of about 40 μm (Figure S7). The CNC film only withstood a weight of 200 g (Figure 5c) and broke under a weight of 500 g (Figure 5d). CNC/PVA-70:30 could withstand a weight of 500 g without failure (Figure 5e) but broke under a weight of 1.0 kg (Figure 5f). It was exciting to find that CNC/PVA-GA could withstand a weight of 1.0 kg (22 421 times of the film weight) and approximately 167 g cm^{-2} without failure and without any crack or fracture (Figure 5g,h), which demonstrated the satisfactory processability of this film. Another benefit of GA cross-linking is an impressive promotion of thermal stability of the CNC composites. Figure S8 shows the thermogravimetric analysis curves of these films. An increase of the temperature at 10% weight loss ($T_{10\%}$) was observed when the pristine CNC ($T_{10\%}$ = 171 °C), CNC/PVA-70:30 ($T_{10\%}$ = 184 °C), and CNC/PVA-GA ($T_{10\%}$ = 238 °C) films were compared. CNC/PVA-GA presented a higher shift temperature in thermal stability. Such an improvement in the mechanical and thermal properties facilitates the development of high-performance CNC-derived photonic materials.

Furthermore, the formation of acetal linkage and an ordered hard/soft nanocomposite structure of the CNC/PVA-GA film was revealed through attenuated total reflection Fourier transform infrared (ATR-FTIR) spectroscopy and atomic force microscopy-based infrared (AFM-IR) spectroscopy analysis.[50−52] ATR-FTIR spectra of the pristine CNC, PVA film, CNC/PVA-70:30, and CNC/PVA-GA films (Figure 6a) display an intense broad band at around 3400 cm^{-1} originating from the O——H stretching vibration and a peak at around

https://doi.org/10.1021/acsami.1c02753
ACS Appl. Mater. Interfaces 2021, 13, 17118−17128

2890 cm^{-1} originating from the C——H stretching vibration of ——CH_2—— groups. The bands at around 1644, 1160, and 1049 cm^{-1} are the characteristic peaks of CNC (Figure 6b), ascribed to the O——H bending, asymmetric C——O——C stretching, and C——O stretching vibrations, respectively.[53,54] The spectra of CNC/PVA-GA show similar bands as CNC rather than PVA because the proportion of CNC was higher than that of PVA. The vibration peak at 1716 cm^{-1} slightly increased, which was ascribed to the unreacted aldehyde.[39,55,56] In comparison with CNC/PVA-70:30, the peak intensity at 3400 cm^{-1} (O——H stretching) and 1440 cm^{-1} (C——OH in-plane bend) of CNC/PVA-GA reduced distinctly, indicating that the dialdehyde group of GA reacted with a large number of hydroxyl groups of CNC and PVA to form the cross-linked network.[57,58]

The AFM-IR technique remarkably increases the spatial resolution of IR spectroscopy to the nanometer, which allows us to probe the spatial distribution of polymorphs, providing more details about the formation of chemical bonds and the chemical composition of the self-assembled nanostructure.[59,60] ATR-FTIR spectra recorded the aldehyde at 1716 cm^{-1} on CNC/PVA-GA (Figure S9), and this peak could be used to image the distribution of CNC/PVA-GA. Mapping of CNC/PVA-70:30 (Figure 6c) and CNC/PVA-GA (Figure 6d) produced two images with different features. Numerous tiny polymeric particles with an average size of 99 nm were distributed randomly on the surface of CNC/PVA-70:30, and only a few of these particles converted into large aggregates, which corresponded to the physical cross-linking between CNC and PVA. By comparison, the surface of CNC/PVA-GA was rough and heterogeneous and many trenches could be detected clearly, which corresponded to the biphasic distribution. We presumed that the GA chemical cross-linking substantially shortened the distances among CNC and PVA chains, resulting in the heterogeneity of the material at the nanoscale. In addition, AFM height images proved the above presumption that many rodlike particles on the surface of the CNC/PVA-70:30 film showed a surface roughness (R_q, root mean square) of 17 nm (Figure 6e). Compared to CNC/PVA-70:30, the R_q value of CNC/PVA-GA decreased to 12 nm (Figure 6f). Meanwhile, the fluctuation of the polymeric films (inset of Figure 6e,f) decreased from 61 to 49 nm approximately, due to the GA cross-linking.

Furthermore, quantum chemistry calculations [i.e., Gaussian, density functional theory (DFT) at the 6-311g level] were conducted to describe the potential binding models between CNC, PVA, and GA.[61] We used Chem3D to construct the starting configurations of CNC, PVA, and GA. Subsequently, the processes of confirmation optimization were completed with the DFT method in the Gaussian 09 program. The binding models of CNC/PVA and CNC/PVA-GA consist of the most stable conformation, according to the rationality of the spatial conformation, the vibration frequency, and the lowest energy. Becke's three-parameter hybrid exchange function with the Lee–Yang–Parr gradient-corrected correlation functional (B3LYP) with 6-311g was adopted for this calculation without any constraint.[62,63] For a physically cross-linked CNC/PVA network, an entangled fragmentation occurred so that the distance of the chains was 2.82 Å. For a GA-cross-linked CNC/PVA network, their chains were packed and increased interaction between each other so that the adjacent distance decreased to 2.29 Å (Figure 6g,h).

Chiral self-assembled CNC films enable circular polarization properties that include circular dichroism and selective left-handed light reflection.[8,64] Thus, we further evaluated the optical activities of the CNC/PVA-GA film. It was found that CNC/PVA-GA retained the capability of the selective reflection of the left-handed circularly polarized light. CNC/PVA-GA taken through a left circular polarizing filter (L-CPF, Figure 7a) appears much uniformly brighter than that taken

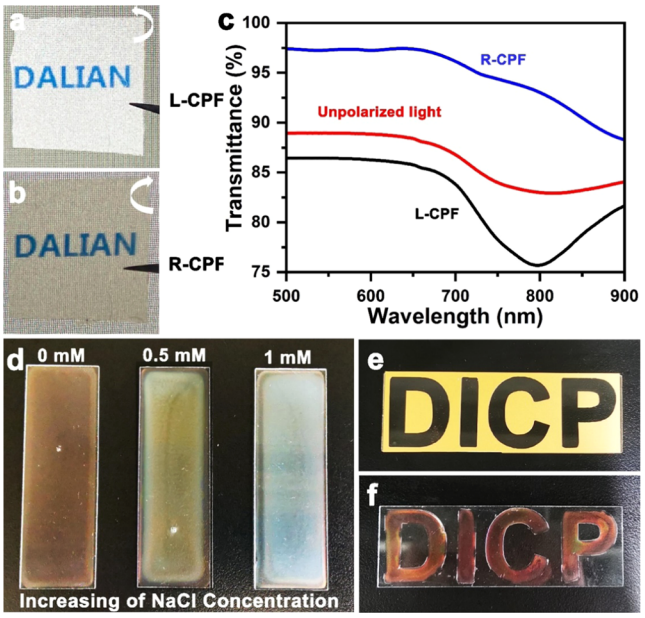

Figure 7. Characterizing optical properties of the CNC/PVA-GA film. (a) Bright or (b) dark films upon incidence of a left (a) or right (b) circular polarizing filter (L- or R-CPF), respectively. (c) Transmission spectra of the CNC/PVA-GA film when light passes through an unpolarized light (red), L-CPF (black), and R-CPF (blue), respectively, recorded using UV–vis spectroscopy. (d) Photographs of CNC/PVA-GA coating on glass slides, in which the tunability of their reflected color was achieved by varying the concentration of NaCl in solution. (e) Hollow "DICP" pattern covering the surface of the glass and subsequent casting of a photonic pattern of the CNC/PVA-GA (f) film.

through a right circular polarizing filter (R-CPF, Figure 7b). To verify this phenomenon, an unpolarized light source is circularly polarized by a filter. The light passes through an unpolarized light, L-CPF, or R-CPF, then through a CNC/PVA-GA film. The intensities of their transmission spectra are recorded using UV–vis spectroscopy. As shown in Figure 7c, a strong transmission peak centered at 800 nm (black line) was observed when the film was irradiated with L-CPF; this peak intensity decreased remarkably (red line) when the unpolarized light was used, and the peak was absent (blue line) when R-CPF was used. These results indicated that CNC/PVA-GA reflected the left-handed circularly polarized light, which was expected since CNC/PVA-GA was inherited from the left-handed structures of chiral nematic CNC.[65]

To develop the full-color coating of the CNC/PVA-GA film, we controlled the reflected color of the films by varying the ionic strength of the solution. Varying the ionic strength of the CNC assembly process is a powerful approach for controlling the reflected color of the iridescent film because the surface sulfate esters on CNCs are sensitive to the ionic strength.[66,67] Three different concentrations (0, 0.5, and 1 mM) of NaCl

https://doi.org/10.1021/acsami.1c02753
ACS Appl. Mater. Interfaces 2021, 13, 17118–17128

(aq) were added to the suspension of CNC/PVA-GA prior to casting the films on glass. As shown in Figure 7d, the three photonic coatings reflected different iridescent colors from red and yellow to blue. When these films were examined using POM, clear birefringence and brilliant colors could be observed (Figure S10). Admirably, CNC/PVA-GA coated on glass was immersed in water and stored for over 2 months under ambient conditions (Figure S11), and its original appearance was well maintained. Combining the evaporation-induced self-assembly strategy with a patterned hollow mask, we can prepare CNC/PVA-GA patterns. In the preparation process, glass was first covered by a poly(vinyl chloride) (PVC) film with a hollow DICP pattern (Figure 6e). CNC/PVA-GA ink was coated onto the unshielded PVC film. After drying and cross-linking, the mask was removed to produce the CNC/PVA-GA pattern (Figure 6f). CNC/PVA-GA was capable of preparing patterns on multiple substrates (Figure S12), including paperboards, polystyrene plastic, rubber, and ceramic. This high-performance CNC composite shows great potential as a cost-effective, long-term stable, and photonic film for the decorative coating that is anticipated to draw widespread attention.

CONCLUSIONS

In summary, a satisfactory photonic CNC nanocomposite film with integrated characteristics, including superb water stability (soaking in water up to 2 months), excellent solvent resistance (tolerance to acid, alkali, and various organic solvents), remarkable mechanical performance (stress up to 113 MPa), and iridescent appearance, was facilely fabricated through a combination of the evaporation-induced self-assembly technique and the effective GA-cross-linking reaction. On the one hand, this strategy provides a facile solution to address the photonic structures of the CNC derivatives incompatible with humid and liquid environments. On the other hand, it addresses the existential dilemma among insolubility, flexibility, and optical activity for the CNC materials. Perhaps predictably, eco-friendly high-end photonics from CNC resources are robust in highly hygroscopic environments. Attributed to these characteristics, the CNC composites function as a versatile platform for future fabrication of multifunctional materials, such as a sustainable polymer in optical signage, smart textile, biological scaffolding, and architectural decoration.

EXPERIMENTAL SECTION

Materials and Characterization. All reagents and solvents including poly(vinyl alcohol) (PVA, 87.0−89.0% hydrolyzed, Aladdin), sulfuric acid (H_2SO_4, 98 wt %), glutaraldehyde (50%), and hydrochloric acid (HCl, 37%) were obtained through standard suppliers. Milli-Q water was used for all experiments. Then, 50 cm polystyrene Petri dishes were supplied by Guangzhou Jet Bio-Filtration Co., Ltd. Seawater is collected from Xinghai Bay, Dalian, Liaoning Province. The suspension of CNCs (2 wt %) was obtained from acid-catalyzed hydrolysis of commercial degreasing cotton, as reported by us previously.[10] Milli-Q water was used for all experiments. UV−vis spectra were measured using a PerkinElmer Lambda 365 spectrophotometer, and circular dichroism (CD) was recorded using a BioTools MOS450 spectropolarimeter. Polarized optical microscopy (POM) images were collected on an Olympus BX53 optical microscope. Infrared (IR) spectra were collected on a Nicolet iS50 spectrometer. Scanning electron microscope (SEM) images were collected on a Carl Zeiss Helium ion microscope. Tensile tests were carried out on an INSTRON 3366 machine at room temperature. The samples were conditioned at 50% RH for 48 h, testing at a nominal strain rate of 1 mm min^{-1} and a gauge length of 10 mm. At least four specimens were tested for each condition. Atomic force microscopy (AFM) images were conducted on NanoWizard ULTRA Speed JPK in QI mode. Atomic force microscopy-infrared (AFM-IR) spectra measurement was performed on an Anasys nanoIR3 system (Bruker). Spectra were collected by mounting films so that the surfaces of the films were perpendicular to the beam path.

Preparation of the CNC/PVA Composite. To obtain optimal flexibility in the CNC/PVA composite films, in a representative procedure, 3 mL of PVA aqueous solution (2 wt % in water) was added to 7 mL of 2 wt % CNC suspension with vigorous stirring. The mixture suspension was stirred for 12 h at room temperature. Then, 1 mL of the portion was transferred into a polystyrene Petri dish (diameter: 25 mm) and dried for 24 h at ambient conditions. To tune the ratios of CNC/PVA from 90:10 to 30:70 (w/w), we adjusted the adding ratio of cellulose and poly(vinyl alcohol) (Table S3). The morphological and physical characteristics of these colorful CNC/PVA films were investigated using a camera, POM, and tensile tests.

Preparation of Water-Stable CNC/PVA-GA and Tunable Iridescence. Briefly, 10 mL of CNC/PVA-70:30 aqueous dispersions were mixed with different volumes of GA (50 wt %), which achieved a GA concentration of 0.5, 1.0, 1.5, and 2.0 wt % in the mixture solutions. The detailed addition amount of GA volume is shown in Table S3. The resulting homogeneous suspension was stirred for 12 h at room temperature. Then, the suspension was poured into polystyrene Petri dishes (diameter: 50 mm) and dried under ambient conditions for 3 days to form composite films. The resulting films showed iridescence. Thereafter, the films were transferred to a beaker (250 mL) containing HCl in a glass vial (5 mL of HCl in a 20 mL vial) for vapor cross-linking during this process, and the beaker was covered with plastic wrap and held for 5 min (Figure S3a). Then, the GA-cross-linked CNC composite films were washed with a copious amount of deionized water. As a result, 0.5, 1.0, and 1.5 wt % GA-cross-linked CNC composites show iridescence observable by the naked eye (Figure S3b−e), while the color of the 2.0 wt % GA-cross-linked composite disappeared. In general, the composites became flexible with an increased amount of GA. Among them, 1.5 wt % GA-cross-linked composites not only showed structural integrity but could also be bent and folded without breaking (Figure S4). Therefore, we chose 1.5 wt % GA-cross-linked composite films (CNC/PVA-GA) as the research object in the subsequent research.

ASSOCIATED CONTENT

Supporting Information

The Supporting Information is available free of charge at https://pubs.acs.org/doi/10.1021/acsami.1c02753.

Pictures and POM images for the CNC/PVA film in different proportions; stability analysis for pristine CNC and CNC/PVA films; thermogravimetric analysis (TGA) curves; stress−strain curves; AFM-IR spectra; SEM image; POM images of CNC/PVA-GA with adjustable structural color; CNC/PVA-GA film patterning on a variety of substrates; and detailed mechanical performance in tables (PDF)

AUTHOR INFORMATION

Corresponding Author

Guangyan Qing − *CAS Key Laboratory of Separation Science for Analytical Chemistry, Dalian Institute of Chemical Physics, Chinese Academy of Sciences, Dalian 116023, P. R. China; University of Chinese Academy of Sciences, Beijing 100049, P. R. China; Key Laboratory of Advanced Energy Materials Chemistry (Ministry of Education), College of Chemistry, Nankai University, Tianjin 300071, P. R. China;*

https://doi.org/10.1021/acsami.1c02753
ACS Appl. Mater. Interfaces 2021, 13, 17118−17128

orcid.org/0000-0002-4888-9318; Email: qinggy@dicp.ac.cn

Authors

Fusheng Zhang − *CAS Key Laboratory of Separation Science for Analytical Chemistry, Dalian Institute of Chemical Physics, Chinese Academy of Sciences, Dalian 116023, P. R. China; University of Chinese Academy of Sciences, Beijing 100049, P. R. China*

Wenna Ge − *School of Mechanical Engineering, Dalian University of Technology, Dalian 116024, P. R. China*

Cunli Wang − *CAS Key Laboratory of Separation Science for Analytical Chemistry, Dalian Institute of Chemical Physics, Chinese Academy of Sciences, Dalian 116023, P. R. China*

Xintong Zheng − *CAS Key Laboratory of Separation Science for Analytical Chemistry, Dalian Institute of Chemical Physics, Chinese Academy of Sciences, Dalian 116023, P. R. China*

Dongdong Wang − *CAS Key Laboratory of Separation Science for Analytical Chemistry, Dalian Institute of Chemical Physics, Chinese Academy of Sciences, Dalian 116023, P. R. China*

Xiancheng Zhang − *CAS Key Laboratory of Separation Science for Analytical Chemistry, Dalian Institute of Chemical Physics, Chinese Academy of Sciences, Dalian 116023, P. R. China*

Xue Wang − *CAS Key Laboratory of Separation Science for Analytical Chemistry, Dalian Institute of Chemical Physics, Chinese Academy of Sciences, Dalian 116023, P. R. China*

Xingya Xue − *CAS Key Laboratory of Separation Science for Analytical Chemistry, Dalian Institute of Chemical Physics, Chinese Academy of Sciences, Dalian 116023, P. R. China; University of Chinese Academy of Sciences, Beijing 100049, P. R. China*

Complete contact information is available at: https://pubs.acs.org/10.1021/acsami.1c02753

Notes

The authors declare no competing financial interest.

■ ACKNOWLEDGMENTS

This work was supported by the National Natural Science Foundation of China (51533007 and 21775116), DICP Innovation Funding (DICP-RC201801), and LiaoNing Revitalization Talents Program (XLYC1802109).

■ REFERENCES

(1) Espinha, A.; Dore, C.; Matricardi, C.; Alonso, M. I.; Goni, A. R.; Mihi, A. Hydroxypropyl Cellulose Photonic Architectures by Soft Nanoimprinting Lithography. *Nat. Photonics* **2018**, *12*, 343−348.

(2) Ogiwara, T.; Katsumura, A.; Sugimura, K.; Teramoto, Y.; Nishio, Y. Calcium Phosphate Mineralization in Cellulose Derivative/Poly(acrylic acid) Composites Having a Chiral Nematic Mesomorphic Structure. *Biomacromolecules* **2015**, *16*, 3959−3969.

(3) Tran, A.; Boott, C. E.; MacLachlan, M. J. Understanding the Self-Assembly of Cellulose Nanocrystals—Toward Chiral Photonic Materials. *Adv. Mater.* **2020**, *32*, No. 1905876.

(4) Thomas, B.; Raj, M. C.; Athira, K. B.; Rubiyah, M. H.; Joy, J.; Moores, A.; Drisko, G. L.; Sanchez, C. Nanocellulose, a Versatile Green Platform: From Biosources to Materials and Their Applications. *Chem. Rev.* **2018**, *118*, 11575−11625.

(5) Gan, L.; Liu, S.; Li, D.; Huang, J. *Nanocellulose: From Fundamentals to Advanced Materials*; Wiley-VCH: Verlag GmbH & Co., KGaA, 2019.

(6) Tran, A.; Hamad, W. Y.; MacLachlan, M. J. Fabrication of Cellulose Nanocrystal Films through Differential Evaporation for Patterned Coatings. *ACS Appl. Nano Mater.* **2018**, *1*, 3098−3104.

(7) Frka-Petesic, B.; Guidetti, G.; Kamita, G.; Vignolini, S. Controlling the Photonic Properties of Cholesteric Cellulose Nanocrystal Films with Magnets. *Adv. Mater.* **2017**, *29*, No. 1701469.

(8) Hiratani, T.; Hamad, W. Y.; MacLachlan, M. J. Transparent Depolarizing Organic and Inorganic Films for Optics and Sensors. *Adv. Mater.* **2017**, *29*, No. 1606083.

(9) Xiong, R.; Yu, S.; Kang, S.; Adstedt, K. M.; Nepal, D.; Bunning, T. J.; Tsukruk, V. V. Integration of Optical Surface Structures with Chiral Nanocellulose for Enhanced Chiroptical Properties. *Adv. Mater.* **2020**, *32*, No. 1905600.

(10) Zhang, F.; Wang, D.; Qin, H.; Feng, L.; Liang, X.; Qing, G. Chemoselectivity of Pristine Cellulose Nanocrystal Films Driven by Carbohydrate−Carbohydrate Interactions. *ACS Appl. Mater. Interfaces* **2019**, *11*, 13114−13122.

(11) Zhao, G.; Zhang, Y.; Zhai, S.; Sugiyama, J.; Pan, M.; Shi, J.; Lu, H. Dual Response of Photonic Films with Chiral Nematic Cellulose Nanocrystals: Humidity and Formaldehyde. *ACS Appl. Mater. Interfaces* **2020**, *12*, 17833−17844.

(12) Grey, P.; Fernandes, S. N.; Gaspar, D.; Fortunato, E.; Martins, R.; Godinho, M. H.; Pereira, L. Field-Effect Transistors on Photonic Cellulose Nanocrystal Solid Electrolyte for Circular Polarized Light Sensing. *Adv. Funct. Mater.* **2019**, *29*, No. 1805279.

(13) Cheng, Z.; Ma, Y.; Yang, L.; Cheng, F.; Huang, Z.; Natan, A.; Li, H.; Chen, Y.; Cao, D.; Huang, Z.; Wang, Y.; Liu, Y.; Yang, R.; Zhu, H. Plasmonic-Enhanced Cholesteric Films: Coassembling Anisotropic Gold Nanorods with Cellulose Nanocrystals. *Adv. Opt. Mater.* **2019**, *7*, No. 1801816.

(14) Chen, J.; Xu, L.; Lin, X.; Chen, R.; Yu, D.; Hong, W.; Zheng, Z.; Chen, X. Self-Healing Responsive Chiral Photonic Films for Sensing and Encoding. *J. Mater. Chem., C* **2018**, *6*, 7767−7775.

(15) Habibi, Y.; Lucia, L. A.; Rojas, O. J. Cellulose Nanocrystals: Chemistry, Self-Assembly, and Applications. *Chem. Rev.* **2010**, *110*, 3479−3500.

(16) Wang, B.; Walther, A. Self-Assembled, Iridescent, Crustacean-Mimetic Nanocomposites with Tailored Periodicity and Layered Cuticular Structure. *ACS Nano* **2015**, *9*, 10637−10646.

(17) Shang, L.; Zhang, W.; Xu, K.; Zhao, Y. Bio-Inspired Intelligent Structural Color Materials. *Mater. Horiz.* **2019**, *6*, 945−958.

(18) Feng, S.; Delannoy, J.; Malod, A.; Zheng, H.; Quéré, D.; Wang, Z. Tip-Induced Flipping of Droplets on Janus Pillars: From Local Reconfiguration to Global Transport. *Sci. Adv.* **2020**, *6*, No. eabb4540.

(19) Pilz da Cunha, M.; Debije, M. G.; Schenning, A. P. H. J. Bioinspired Light-Driven Soft Robots Based on Liquid Crystal Polymers. *Chem. Soc. Rev.* **2020**, *49*, 6568−6578.

(20) Wang, Z.; Wang, S.; Huang, L.; Li, L.; Chi, L. Microstructured Ultrathin Organic Semiconductor Film via Dip-Coating: Precise Assembly and Diverse Applications. *Acc. Mater. Res.* **2020**, *1*, 201−212.

(21) Teyssier, J.; Saenko, S. V.; van der Marel, D.; Milinkovitch, M. C. Photonic Crystals Cause Active Colour Change in Chameleons. *Nat. Commun.* **2015**, *6*, No. 6368.

(22) Lee, G. H.; Choi, T. M.; Kim, B.; Han, S. H.; Lee, J. M.; Kim, S.-H. Chameleon-Inspired Mechanochromic Photonic Films Composed of Non-Close-Packed Colloidal Arrays. *ACS Nano* **2017**, *11*, 11350−11357.

(23) Xiong, R.; Yu, S.; Smith, M. J.; Zhou, J.; Krecker, M.; Zhang, L.; Nepal, D.; Bunning, T. J.; Tsukruk, V. V. Self-Assembly of Emissive Nanocellulose/Quantum Dot Nanostructures for Chiral Fluorescent Materials. *ACS Nano* **2019**, *13*, 9074−9081.

(24) Xu, M.; Wu, X.; Yang, Y.; Ma, C.; Li, W.; Yu, H.; Chen, Z.; Li, J.; Zhang, K.; Liu, S. Designing Hybrid Chiral Photonic Films with Circularly Polarized Room-Temperature Phosphorescence. *ACS Nano* **2020**, *14*, 11130−11139.

(25) Khan, M. K.; Hamad, W. Y.; MacLachlan, M. J. Tunable Mesoporous Bilayer Photonic Resins with Chiral Nematic Structures and Actuator Properties. *Adv. Mater.* **2014**, *26*, 2323−2328.

(26) Liu, Y.; Wu, P. Bioinspired Hierarchical Liquid-Metacrystal Fibers for Chiral Optics and Advanced Textiles. *Adv. Funct. Mater.* **2020**, *30*, No. 2002193.
(27) Yao, K.; Meng, Q.; Bulone, V.; Zhou, Q. Flexible and Responsive Chiral Nematic Cellulose Nanocrystal/Poly(ethylene glycol) Composite Films with Uniform and Tunable Structural Color. *Adv. Mater.* **2017**, *29*, No. 1701323.
(28) Sui, Y.; Li, X.; Chang, W.; Wan, H.; Li, W.; Yang, F.; Yu, Z. Z. Multi-Responsive Nanocomposite Membranes of Cellulose Nanocrystals and Poly(N-isopropyl acrylamide) with Tunable Chiral Nematic Structures. *Carbohydr. Polym.* **2020**, *232*, No. 115778.
(29) Kose, O.; Tran, A.; Lewis, L.; Hamad, W. Y.; MacLachlan, M. J. Unwinding a Spiral of Cellulose Nanocrystals for Stimuli-Responsive Stretchable Optics. *Nat. Commun.* **2019**, *10*, No. 510.
(30) Vollick, B.; Kuo, P.-Y.; Thérien-Aubin, H.; Yan, N.; Kumacheva, E. Composite Cholesteric Nanocellulose Films with Enhanced Mechanical Properties. *Chem. Mater.* **2017**, *29*, 789−795.
(31) Moon, R. J.; Martini, A.; Nairn, J.; Simonsen, J.; Youngblood, J. Cellulose Nanomaterials Review: Structure, Properties and Nanocomposites. *Chem. Soc. Rev.* **2011**, *40*, 3941−3994.
(32) Kontturi, E.; Laaksonen, P.; Linder, M. B.; Nonappa; Gröschel, A. H.; Rojas, O. J.; Ikkala, O. Advanced Materials through Assembly of Nanocelluloses. *Adv. Mater.* **2018**, *30*, No. 1703779.
(33) Kawai, F.; Hu, X. Biochemistry of Microbial Polyvinyl Alcohol Degradation. *Appl. Microbiol. Biotechnol.* **2009**, *84*, 227−237.
(34) Song, P.; Xu, Z.; Dargusch, M. S.; Chen, Z.-G.; Wang, H.; Guo, Q. Granular Nanostructure: A Facile Biomimetic Strategy for the Design of Supertough Polymeric Materials with High Ductility and Strength. *Adv. Mater.* **2017**, *29*, No. 1704661.
(35) Sharma, R.; Tiwari, S.; Tiwari, S. K. Highly Reflective Nanostructured Titania Shell: A Sustainable Pigment for Cool Coatings. *ACS Sustainable Chem. Eng.* **2018**, *6*, 2004−2010.
(36) Yuan, W.; Li, Q.; Zhou, N.; Zhang, S.; Ding, C.; Shi, L.; Zhang, K.-Q. Structural Color Fibers Directly Drawn from Colloidal Suspensions with Controllable Optical Properties. *ACS Appl. Mater. Interfaces* **2019**, *11*, 19388−19396.
(37) Clough, J. M.; Guimard, E.; Rivet, C.; Sprakel, J.; Kodger, T. E. Photonic Paints: Structural Pigments Combined with Water-Based Polymeric Film-Formers for Structurally Colored Coatings. *Adv. Opt. Mater.* **2019**, *7*, No. 1900218.
(38) Parker, R. M.; Guidetti, G.; Williams, C. A.; Zhao, T.; Narkevicius, A.; Vignolini, S.; Frka-Petesic, B. The Self-Assembly of Cellulose Nanocrystals: Hierarchical Design of Visual Appearance. *Adv. Mater.* **2018**, *30*, No. 1704477.
(39) Destaye, A. G.; Lin, C.-K.; Lee, C.-K. Glutaraldehyde Vapor Cross-linked Nanofibrous PVA Mat with in Situ Formed Silver Nanoparticles. *ACS Appl. Mater. Interfaces* **2013**, *5*, 4745−4752.
(40) Chen, M.; Chen, J.; Zhou, W.; Xu, J.; Wong, C.-P. High-Performance Flexible and Self-Healable Auasi-Solid-State Ainc-Ion Hybrid Supercapacitor Based on Borax-Crosslinked Polyvinyl Alcohol/Nanocellulose Hydrogel Electrolyte. *J. Mater. Chem. A* **2019**, *7*, 26524−26532.
(41) de Vries, H. Rotatory Power and Other Optical Properties of Certain Liquid Crystals. *Acta Crystallogr.* **1951**, *4*, 219−226.
(42) Shopsowitz, K. E.; Qi, H.; Hamad, W. Y.; Maclachlan, M. J. Free-Standing Mesoporous Silica Films with Tunable Chiral Nematic Structures. *Nature* **2010**, *468*, 422−425.
(43) Lemke, C. H.; Dong, R. Y.; Michal, C. A.; Hamad, W. Y. New Insights into Nano-Crystalline Cellulose Structure and Morphology Based on Solid-State NMR. *Cellulose* **2012**, *19*, 1619−1629.
(44) Giese, M.; Blusch, L. K.; Khan, M. K.; Hamad, W. Y.; MacLachlan, M. J. Responsive Mesoporous Photonic Cellulose Films by Supramolecular Cotemplating. *Angew. Chem., Int. Ed.* **2014**, *53*, 8880−8884.
(45) Xu, M.; Li, W.; Ma, C.; Yu, H.; Wu, Y.; Wang, Y.; Chen, Z.; Li, J.; Liu, S. Multifunctional Chiral Nematic Cellulose Nanocrystals/Glycerol Structural Colored Nanocomposites for Intelligent Responsive Films, Photonic Inks and Iridescent Coatings. *J. Mater. Chem. C* **2018**, *6*, 5391−5400.
(46) d'Eon, J.; Zhang, W.; Chen, L.; Berry, R. M.; Zhao, B. X. Coating Cellulose Nanocrystals on Polypropylene and Its Film Adhesion and Mechanical Properties. *Cellulose* **2017**, *24*, 1877−1888.
(47) Walters, C. M.; Boott, C. E.; Nguyen, T.-D.; Hamad, W. Y.; MacLachlan, M. J. Iridescent Cellulose Nanocrystal Films Modified with Hydroxypropyl Cellulose. *Biomacromolecules* **2020**, *21*, 1295−1302.
(48) Adstedt, K.; Popenov, E. A.; Pierce, K. J.; Xiong, R.; Geryak, R.; Cherpak, V.; Nepal, D.; Bunning, T. J.; Tsukruk, V. V. Chiral Cellulose Nanocrystals with Intercalated Amorphous Polysaccharides for Controlled Iridescence and Enhanced Mechanics. *Adv. Funct. Mater.* **2020**, *30*, No. 2003597.
(49) Tu, H.; Zhu, M.; Duan, B.; Zhang, L. Recent Progress in High-Strength and Robust Regenerated Cellulose Materials. *Adv. Mater.* **2020**, *51*, No. 2000682.
(50) Lahiri, B.; Holland, G.; Centrone, A. Chemical Imaging Beyond the Diffraction Limit: Experimental Validation of the PTIR Technique. *Small* **2013**, *9*, 439−445.
(51) Nasse, M. J.; Walsh, M. J.; Mattson, E. C.; Reininger, R.; Kajdacsy-Balla, A.; Macias, V.; Bhargava, R.; Hirschmugl, C. J. High-Resolution Fourier-Transform Infrared Chemical Imaging with Multiple Synchrotron Beams. *Nat. Methods* **2011**, *8*, 413−416.
(52) Marcott, C.; Lo, M.; Kjoller, K.; Prater, C.; Noda, I. Spatial Differentiation of Sub-Micrometer Domains in a Poly-(hydroxyalkanoate) Copolymer Using Instrumentation that Combines Atomic Force Microscopy (AFM) and Infrared (IR) Spectroscopy. *Appl. Spectrosc.* **2011**, *65*, 1145−1150.
(53) Hu, W.; Liu, S.; Chen, S.; Wang, H. Preparation and Properties of Photochromic Bacterial Cellulose Nanofibrous Membranes. *Cellulose* **2011**, *18*, 655−661.
(54) Han, J.; Zhou, C.; Wu, Y.; Liu, F.; Wu, Q. Self-Assembling Behavior of Cellulose Nanoparticles during Freeze-Drying: Effect of Suspension Concentration, Particle Size, Crystal Structure, and Surface Charge. *Biomacromolecules* **2013**, *14*, 1529−1540.
(55) Zhu, H.; Narakathu, B. B.; Fang, Z.; Tausif Aijazi, A.; Joyce, M.; Atashbar, M.; Hu, L. A Gravure Printed Antenna on Shape-Stable Transparent Nanopaper. *Nanoscale* **2014**, *6*, 9110−9115.
(56) Kumar, A.; Ryparová, P.; Hosseinpourpia, R.; Adamopoulos, S.; Prošek, Z.; Žigon, J.; Petrič, M. Hydrophobicity and Resistance Against Microorganisms of Heat and Chemically Crosslinked Poly(vinyl alcohol) Nanofibrous Membranes. *Chem. Eng. J. 360*, 788 796. DOI: 10.1016/j.cej.2018.12.029.
(57) Mansur, H. S.; Sadahira, C. M.; Souza, A. N.; Mansur, A. A. P. FTIR Spectroscopy Characterization of Poly(vinyl alcohol) Hydrogel with Different Hydrolysis Degree and Chemically Crosslinked with Glutaraldehyde. *Mater. Sci. Eng., C* **2008**, *28*, 539−548.
(58) Rimdusit, S.; Somsaeng, K.; Kewsuwan, P.; Jubsilp, C.; Tiptipakorn, S. Comparison of Gamma Radiation Crosslinking and Chemical Crosslinking on Properties of Methylcellulose Hydrogel. *Eng. J.* **2012**, *16*, 15−28.
(59) Tang, F.; Bao, P.; Su, Z. Analysis of Nanodomain Composition in High-Impact Polypropylene by Atomic Force Microscopy-Infrared. *Anal. Chem.* **2016**, *88*, 4926−4930.
(60) Kim, S. Y.; Khanal, D.; Kalionis, B.; Chrzanowski, W. High-Fidelity Probing of the Structure and Heterogeneity of Extracellular Vesicles by Resonance-Enhanced Atomic Force Microscopy Infrared Spectroscopy. *Nat. Protoc.* **2019**, *14*, 576−593.
(61) Frisch, M. J.; Trucks, G. W.; Schlegel, H. B.; Scuseria, G. E.; Robb, M. A.; Cheeseman, J. R.; Scalmani, G.; Barone, V.; Mennucci, B.; Petersson, G. A.; Nakatsuji, H.; Caricato, M.; Li, X.; Hratchian, H. P.; Izmaylov, A. F.; Bloino, J.; Zheng, G.; Sonnenberg, J. L.; Hada, M.; Ehara, M.; Toyota, K.; Fukuda, R.; Hasegawa, J.; Ishida, M.; Nakajima, T.; Honda, Y.; Kitao, O.; Nakai, H.; Vreven, T.; Montgomery, J. A., Jr.; Peralta, J. E.; Ogliaro, F.; Bearpark, M.; Heyd, J. J.; Brothers, E.; Kudin, K. N.; Staroverov, V. N.; Keith, T.; Kobayashi, R.; Normand, J.; Raghavachari, K.; Rendell, A.; Burant, J. C.; Iyengar, S. S.; Tomasi, J.; Cossi, M.; Rega, N.; Millam, J. M.; Klene, M.; Knox, J. E.; Cross, J. B.; Bakken, V.; Adamo, C.; Jaramillo, J.; Gomperts, R.; Stratmann, R. E.; Yazyev, O.; Austin, A. J.; Cammi,

R.; Pomelli, C.; Ochterski, J. W.; Martin, R. L.; Morokuma, K.; Zakrzewski, V. G.; Voth, G. A.; Salvador, P.; Dannenberg, J. J.; Dapprich, S.; Daniels, A. D.; Farkas, O.; Foresman, J. B.; Ortiz, J. V.; Cioslowski, J.; Fox, D. J. *Gaussian 09*, revision C.01; Gaussian Inc.: Wallingford, CT, 2009.

(62) Miehlich, B.; Savin, A.; Stoll, H.; Preuss, H. Results Obtained with the Correlation Energy Density Functionals of Becke and Lee, Yang and Parr. *Chem. Phys. Lett.* **1989**, *157*, 200−206.

(63) Ilic, S.; Alherz, A.; Musgrave, C. B.; Glusac, K. D. Thermodynamic and Kinetic Hydricities of Metal-Free Hydrides. *Chem. Soc. Rev.* **2018**, *47*, 2809−2836.

(64) Tao, J.; Zou, C.; Jiang, H.; Li, M.; Lu, D.; Mann, S.; Xu, Y. Optically Ambidextrous Reflection and Luminescence in Self-Organized Left-Handed Chiral Nematic Cellulose Nanocrystal Films. *CCS Chem.* **2020**, *2*, 932−945.

(65) Zhang, F.; Zheng, X.; Wang, C.; Wang, D.; Xue, X.; Qing, G. Synthesis of Optically Active Chiral Mesoporous Molybdenum Carbide Film. *J. Ind. Eng. Chem.* **2021**, *94*, 482−488.

(66) Dong, X. M.; Kimura, T.; Revol, J.-F.; Gray, D. G. Effects of Ionic Strength on the Isotropic-Chiral Nematic Phase Transition of Suspensions of Cellulose Crystallites. *Langmuir* **1996**, *12*, 2076−2082.

(67) Giese, M.; Blusch, L. K.; Khan, M. K.; MacLachlan, M. J. Functional Materials from Cellulose-Derived Liquid-Crystal Templates. *Angew. Chem., Int. Ed.* **2015**, *54*, 2888−2910.

https://doi.org/10.1021/acsami.1c02753
ACS Appl. Mater. Interfaces 2021, 13, 17118−17128